Hindawi
Complexity
Volume 2020, Article ID 2624547, 15 pages
https://doi.org/10.1155/2020/2624547

Research Article

Displacement Prediction of a Complex Landslide in the Three Gorges Reservoir Area (China) Using a Hybrid Computational Intelligence Approach

Junwei Ma,[1] **Xiaoxu Niu**,[1] **Huiming Tang**,[1,2] **Yankun Wang**,[2] **Tao Wen**,[3] **and Junrong Zhang**[2]

[1]*Three Gorges Research Center for Geo-Hazards of the Ministry of Education, China University of Geosciences, Wuhan, Hubei 430074, China*
[2]*Faculty of Engineering, China University of Geosciences, Wuhan, Hubei 430074, China*
[3]*School of Geosciences, Yangtze University, Wuhan, Hubei 430100, China*

Correspondence should be addressed to Junwei Ma; majw@cug.edu.cn and Huiming Tang; tanghm@cug.edu.cn

Received 30 August 2019; Revised 17 December 2019; Accepted 8 January 2020; Published 28 January 2020

Academic Editor: Átila Bueno

Displacement prediction of reservoir landslide remains inherently uncertain since a complete understanding of the complex nonlinear, dynamic landslide system is still lacking. An appropriate quantification of predictive uncertainties is a key underpinning of displacement prediction and mitigation of reservoir landslide. A density prediction, offering a full estimation of the probability density for future outputs, is promising for quantification of the uncertainty of landslide displacement. In the present study, a hybrid computational intelligence approach is proposed to build a density prediction model of landslide displacement and quantify the associated predictive uncertainties. The hybrid computational intelligence approach consists of two steps: first, the input variables are selected through copula analysis; second, kernel-based support vector machine quantile regression (KSVMQR) is employed to perform density prediction. The copula-KSVMQR approach is demonstrated through a complex landslide in the Three Gorges Reservoir Area (TGRA), China. The experimental study suggests that the copula-KSVMQR approach is capable of construction density prediction by providing full probability density distributions of the prediction with perfect performance. In addition, different types of predictions, including interval prediction and point prediction, can be derived from the obtained density predictions with excellent performance. The results show that the mean prediction interval widths of the proposed approach at ZG287 and ZG289 are 27.30 and 33.04, respectively, which are approximately 60 percent lower than that obtained using the traditional bootstrap-extreme learning machine-artificial neural network (Bootstrap-ELM-ANN). Moreover, the obtained point predictions show great consistency with the observations, with correlation coefficients of 0.9998. Given the satisfactory performance, the presented copula-KSVMQR approach shows a great ability to predict landslide displacement.

1. Introduction

As one of the most geohazard prone and complex areas, the Three Gorges Reservoir Area (TGRA) suffers from reservoir landslide disasters. Movement and failure of reservoir landslide can result in major economic damage and loss of life. Displacement prediction has been proven to be the most cost-saving risk reduction measure [1] and has been widely applied in landslide early warning and mitigation in TGRA. However, displacement prediction of reservoir landslide remains a key fundamental challenge. This challenge arises due to the inherent geological and mechanical complexity [2] of landslide systems with a large volume (up to millions of cubic meters) of heterogeneous materials. It is widely acknowledged among researchers and practitioners that properties of landslide materials vary spatially exhibiting heterogeneous features [3, 4]. Furthermore, previous studies have proven that reservoir landslide is a complex nonlinear dynamic system [5], and movement and failure may be induced by combined and

periodic effects of heavy rainfall and reservoir fluctuations [6, 7].

Since the pioneering work of Saito [8], a number of models, including deterministic models, statistical models, and computational intelligence-based models, have been proposed to build prediction models for landslide displacement [9]. Recently, due to advantages of speed and precision, computer intelligence techniques have been widely used in landslide displacement prediction. The computational intelligence-based models include, but are not limited to, the artificial neural network (ANN) [10], extreme learning machines (ELM) [11], and the support vector machine (SVM) [1, 12–14]. Recently, deep learning models [15, 16] and hybrid models based on time series decomposition and computational intelligence techniques [11, 17] have become popular in landslide displacement prediction.

Although amenable to a large number of applications, many researchers have shown that the establishment of a computer intelligence-based model is inherently stochastic, as identical results would be difficult to reproduce on different occasions [18–21]. Such characteristics may seriously weaken the reliability of computer intelligence-based models. Moreover, computer intelligence-based deterministic point prediction is of limited value when uncertainties are present [22].

In fact, a complete understanding of this nonlinear dynamic landslide system is lacking, which causes significant uncertainties in landslide displacement prediction [5, 23]. Therefore, significant effort is needed to address these predictive uncertainties associated with computer intelligence outputs, thus building a reliable landslide prediction model. However, only a few studies have been reported on prediction and uncertainty quantification of landslide displacement. A novel neural network with random hidden weights was proposed by Lian et al. [24] to quantify the uncertainties in landslide displacement prediction and construct a prediction interval (PI) at a certain nominal probability $(1-\alpha)\times 100\%$, which is named the PI nominal confidence (PINC). A hybrid approach based on an echo state network and mean-variance estimation was proposed by Yao et al. [25] to measure the uncertainties in landslide displacement prediction and construct a PI at a specific probability. A hybrid intelligent approach using double exponential smoothing, particle swarm optimization, and extreme machine learning (DES-PSO-ELM) was proposed by Wang et al. [26] to construct lower and upper bound estimation- (LUBE-) based PIs.

However, to our best knowledge, the prediction models accounting for uncertainties that are available today for landslide displacement prediction only concentrate on a specific nominal probability or confidence level. Different from those aforementioned models, density prediction conveys more information by constructing a full probability density distribution of predictive displacement rather than a specified confidence level. In this study, a hybrid computational intelligence approach using a copula and kernel-based support vector machine quantile regression (copula-KSVMQR) was proposed to build a density prediction model and quantify the associated predictive uncertainties. A complex landslide in the TGRA has been chosen as a case study to explore the performance of the hybrid copula-KSVMQR approach.

2. Methodology

2.1. Density Prediction. According to output type, landslide displacement predictions can be divided into the following three categories: point prediction, interval prediction, and density prediction (schematic illustrated in Figure 1). The output of a point prediction is a single number. A good point prediction provides a simple and easily understandable guide to future outputs. However, point prediction can only be helpful when no significant uncertainties are involved. Such unpredictable shocks affect all of the predictive outputs. As a result of such shocks, we expect a nonzero prediction error, even from very good predictions. Thus, we must determine the degree of confidence or uncertainty associated with a particular point prediction. The uncertainties associated with point prediction suggest the usefulness of an interval prediction.

The output of an interval prediction is not a single number; rather, interval prediction provides lower and upper bounds between which the future event is expected to fall within a predefined probability. Compared with point prediction, interval prediction has several potential benefits. First, the widths of constructed PIs convey information regarding prediction uncertainties; in contrast, such information is unavailable in point prediction. Second, given an interval prediction, a point prediction can be derived using the midpoint of the constructed interval. Conversely, given only a point prediction, there is no way to infer an interval prediction.

A density prediction gives a full estimation of the probability density for future outputs. As with interval prediction, density prediction provides more information than interval prediction, with the ability to derive a point prediction from a median prediction and construct any desired confidence level.

2.2. Copula. The copula [27] is a statistical technique connecting multivariate distribution functions to their one-dimensional marginal distribution functions [28]. It has been widely applied to identify correlation relationships in the fields of energy, river runoff, crude oil prices, and geotechnics [29–34].

Given random variables x and y with marginal cumulative distribution functions $F(x)$ and $F(y)$, there exists a unique copula function C that satisfies the expression

$$H(x,y) = C\left(F(x), F(y); \theta, \rho_{xy}\right), \tag{1}$$

where $H(x,y)$ is the joint cumulative distribution function, θ is the copula parameter, and ρ_{xy} is the correlation measure between random variables x and y. The marginal probability density function $f(x)$ of variable x can be obtained using Gaussian kernel density estimation as [35]

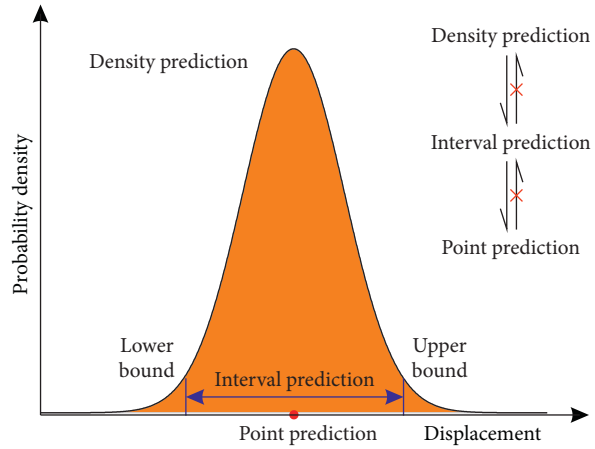

FIGURE 1: Schematic diagram of point prediction, interval prediction, and density prediction.

$$\widehat{f}_h(x) = \frac{1}{nh}\sum_{i=1}^{n} K\left(\frac{x - x_i}{h}\right) = \frac{1}{nh}\sum_{i=1}^{n} \frac{1}{\sqrt{2\pi}} \exp\left[-\frac{(x - x_i)^2}{2h^2}\right], \tag{2}$$

where h is the bandwidth and n is the sample size of variable x.

Gaussian copula, Student's t copula, Clayton copula, Frank copula, and Gumbel copula are commonly used copula functions. In this study, Student's t copula was adopted due to its strong ability to capture extreme values [36]. Kendall's Tau and Spearman's Rho, with values between −1 and +1, are widely used to measure the nonlinear correlation between random variables. A positive value indicates a positive correlation, whereas a negative value represents a reverse correlation. The absolute value of the correlation coefficient indicates the strength of the correlation. Based on the most commonly used interpretation provided by Quinnipiac University [37, 38], the strength of the correlation can be interpreted as follows: an absolute value greater than 0.7 demonstrates a very strong correlation, an absolute value from 0.3 to 0.7 shows a strong correlation, an absolute value from 0.2 to 0.3 represents a moderate correlation, an absolute value between 0.1 and 0.2 demonstrates a weak correlation, and an absolute value less than 0.1 indicates a negligible correlation. Variables with a negligible correlation could be ignored during modeling. Therefore, the variables showing weak to very strong correlations, with absolute values greater than 0.1 [39], were selected as the input variables in this study.

2.3. Kernel-Based Support Vector Machine Quantile Regression (KSVMQR)

2.3.1. Quantile Regression (QR). For any real-valued random variable, Y may be characterized by its (right-continuous) distribution function

$$F(Y) = P(Y \le y), \tag{3}$$

while for any $0 < \tau < 1$,

$$F^{-1}(\tau) = \inf\{y: F(y) \ge \tau\} \tag{4}$$

is called the τth quantile of Y.

Quantile regression (QR) was first introduced by Koenker and Bassett [40] to replace the traditional mean regression. It provides a complete picture for the entire conditional distribution of a response variable y when x is an explanatory variable instead of the conditional mean only [41]. Consider a data set $(x_t, y_t)_{t=1}^{T}$, where x_t is a $k \times 1$ vector of regression. The quantile regression can be expressed as

$$y_t = x_t^T \beta(\tau) + \varepsilon_t(\tau), \quad t = 1, 2, \ldots, T, \tag{5}$$

where $x_t = (1, x_{t,1}, x_{t,2}, \ldots, x_{t,k})'$, $\beta_\tau = (\beta_0(\tau), \beta_1(\tau), \beta_2(\tau), \ldots, \beta_k(\tau))'$, $0 < \tau < 1$ is the quantile, and $\varepsilon_t(\tau)$ is an error with a zero expectation. The estimated parameters $\beta(\tau)$ can be approximated through minimizing a sum of asymmetrically weighted absolute residual cost functions, expressed as

$$\min_{\beta} \sum_{t=1}^{T} \rho_\tau\left(y_t - x_t^T \beta\right), \tag{6}$$

where ρ_τ is the check function, also known as the pinball loss function, and defined as follows:

$$\rho_\tau(x) = \begin{cases} \tau x, & \text{if } x \ge 0, \\ (\tau - 1)x, & \text{if } x < 0. \end{cases} \tag{7}$$

The median case, $\tau = 0.5$, which is equivalent to minimizing the sum of the absolute values, is usually known as median regression or least absolute value regression.

2.3.2. Kernel-Based Support Vector Machine (KSVM). An SVM [42] is a supervised learning method initially designed for pattern recognition. Recently, SVMs have widely been used for regression [43, 44] by applying a cost function, e.g., ε-insensitive loss function, to measure the empirical risk in order to minimize the regression error. When tackling the problems of regression, the SVM approach is also referred to as support vector regression (SVR). The key features of SVMs are the use of kernels [45], so expert knowledge can be built in by engineering the kernel. Additional, SVMs retain the advantage of the absence of local minima.

Given a data set $(x_t, y_t)_{t=1}^{T}$, the linear regression model can be expressed as

$$\widehat{y}_t = f(x_t) = \omega \cdot \phi(x_t) + b, \tag{8}$$

where ω, $\phi(\cdot)$, and b are the weight vector, nonlinear mapping function, and threshold, respectively. The optimal parameters (ω, b) of an SVM model can be obtained by solving the optimization equation:

$$\min_{\omega,b} \frac{1}{2}\|\omega\|^2 + C\sum_{t=1}^{T}\left|\xi_t + \xi_t^*\right|, \tag{9}$$

where C is a penalty parameter and ξ_t and ξ_t^* are slack variables introduced to evaluate the deviation of training samples outside the ε-insensitive zone.

KSVM is an algorithm that applies kernel functions into the linear SVM. KSVM has the ability to solve nonlinear regression problems with a linear method in the feature space using the ε-insensitive loss function [46] (schematic illustrated in Figure 2). The most popular kernel functions are listed in Table 1.

2.3.3. KSVMQR. A KSVMQR model is implemented by the combination of KSVM and QR, by replacing the penalty function in equation (9) with QR check function in equation (6), and expressed as follows:

$$\min_{\omega_\tau, b_\tau} \frac{1}{2}\|\omega_\tau\|^2 + C\sum_{t=1}^{T}\rho_\tau\left(y_t - b_\tau - \beta_\tau^T\mu_t - \omega_\tau^T\phi(x_t)\right). \quad (10)$$

The above equation can be rewritten as a quadratic programming problem as follows:

$$\begin{aligned} \min \quad & \frac{1}{2}w^T w + C\sum_{t=1}^{T}\left(\tau\xi_t + (1-\tau)\xi_t^*\right) \\ \text{subject to} \quad & \begin{cases} y_t - b - \beta^T z_t - w^T\phi(x_t) \le \xi_t \\ -y_t + b + \beta^T z_t + w^T\phi(x_t) \le \xi_t^* \\ \xi_t, \xi_t^* \ge 0. \end{cases} \end{aligned} \quad (11)$$

The estimators of the KSVMQR can be solved by introduction of slack variables and construction of the Lagrange function as follows:

$$\begin{cases} \omega_\tau = \sum_{t=1}^{T}(\chi_t - \chi_t^*)\phi(x_t), \\ (b_\tau, \beta_\tau)^T = (U^T U)^{-1}U^T(y - K(\chi - \chi^*)), \\ Q_{y_t}\left(\tau \mid u_t, x_t, \eta\right) = b_\tau + \beta_\tau^T u_t + K_t(\chi - \chi^*), \end{cases} \quad (12)$$

where T is the sample size, χ and χ^* denote the optimal Lagrange multiplier, $K(\cdot)$ is the kernel matrix, and $K_t(\cdot)$ is the tth array of the kernel matrix.

2.4. Landslide Displacement Prediction Based on Copula-KSVMQR. The overall framework for the landslide displacement prediction using the copula-KSVMQR approach is shown in Figure 3. It mainly consists of the following stages: (1) correlation assessment, (2) KSVMQR modeling, and (3) interval and point estimation.

2.4.1. Correlation Assessment. The selection of the input variables is essential for the accurate prediction of the landslide displacement. However, as listed in Table 2, in most cases, the input variables were selected based on experience, qualitative analysis, or a literature review, thus leading to insufficient persuasiveness. It is rational and meaningful to use a quantitative method to choose the input variables for landslide displacement prediction. A few studies have tried to choose the input variables based on a grey correlation analysis (GRA). However, GRA suffers the limitations of a strong subjectivity and inability to measure negative correlations [49, 50]. To efficiently improve the selection of the inputs for landslide displacement prediction, in this study, the copula was introduced to estimate the correlation relationship between causal factors and landslide displacement, thus aiding in the selection of input variables.

2.4.2. KSVMQR Modeling. Assume $\widehat{y}_t^{\tau_j}$ is an estimate of the quantile prediction for quantile τ_j at time t. A nonparametric density prediction $\widehat{f}_t$ can be approximated by the joint consideration of a finite number of conditional quantities $(\tau_j)_{j=1}^{J}$ [51, 52]:

$$\widehat{f}_t = \left\{\widehat{y}_t^{\tau_j} \,\middle|\, 0 < \tau_1 \le \cdots \le \tau_j \le \cdots \le \tau_J < 1\right\}. \quad (13)$$

2.4.3. Interval and Point Estimation. A PI gives an interval, consisting of upper and lower bounds, within which we expect y_t to lie with a specified probability. Once quantile predictions and predictive densities are generated, PIs, allowing direct visualization of the uncertainties associated with landslide displacement prediction, are a natural side product. Central PIs with nominal coverage $(1-\alpha)\times 100\%$ can be obtained from quantile predictions $y_t^{\overline{\tau}=1-\alpha/2}$ and $y_t^{\underline{\tau}=\alpha/2}$ $(\overline{\tau} > \underline{\tau})$ at time t as

$$PI_t^{1-\alpha} = \left[y_t^{\underline{\tau}=\alpha/2}, y_t^{\overline{\tau}=1-\alpha/2}\right], \quad (14)$$

where α, also denoting the significance level, refers to the probability of miss-capturing the value of the parameter and $y_t^{\overline{\tau}=1-\alpha/2}$ and $y_t^{\underline{\tau}=\alpha/2}$ correspond to the upper and lower bounds at time t, respectively. For example, a 90% central PI can be obtained from the 0.05 and 0.95 quantile predictions [53].

PIs provide direct visualization of associated uncertainties; however, a quantitative point prediction $(\widehat{y}_t)$ is still needed for decision making in landslide early warning and mitigation. In this study, the median prediction $(\widehat{y}_t^{\tau=0.5})$ measuring the average estimation is used to generate a quantitative input for certain scenarios.

2.5. Evaluation Metrics. In this study, the PI coverage probability (PICP) and average coverage error (ACE) were used to assess the performance of the copula-KSVMQR approach. The PICP reflects the probability that the targets lie within the constructed PI and is defined as follows:

$$\text{PICP} = \frac{1}{T}\sum_{t=1}^{T} I_t^{1-\alpha}, \quad (15)$$

where T is the sample size. $I_t^{1-\alpha}$ is defined as follows:

$$I_t^{1-\alpha} = \begin{cases} 1, & y_t \in \left[y_t^{\underline{\tau}}, y_t^{\overline{\tau}}\right], \\ 0, & y_t \notin \left[y_t^{\underline{\tau}}, y_t^{\overline{\tau}}\right]. \end{cases} \quad (16)$$

The ACE represents the deviation of PICP from PINC and is defined as follows:

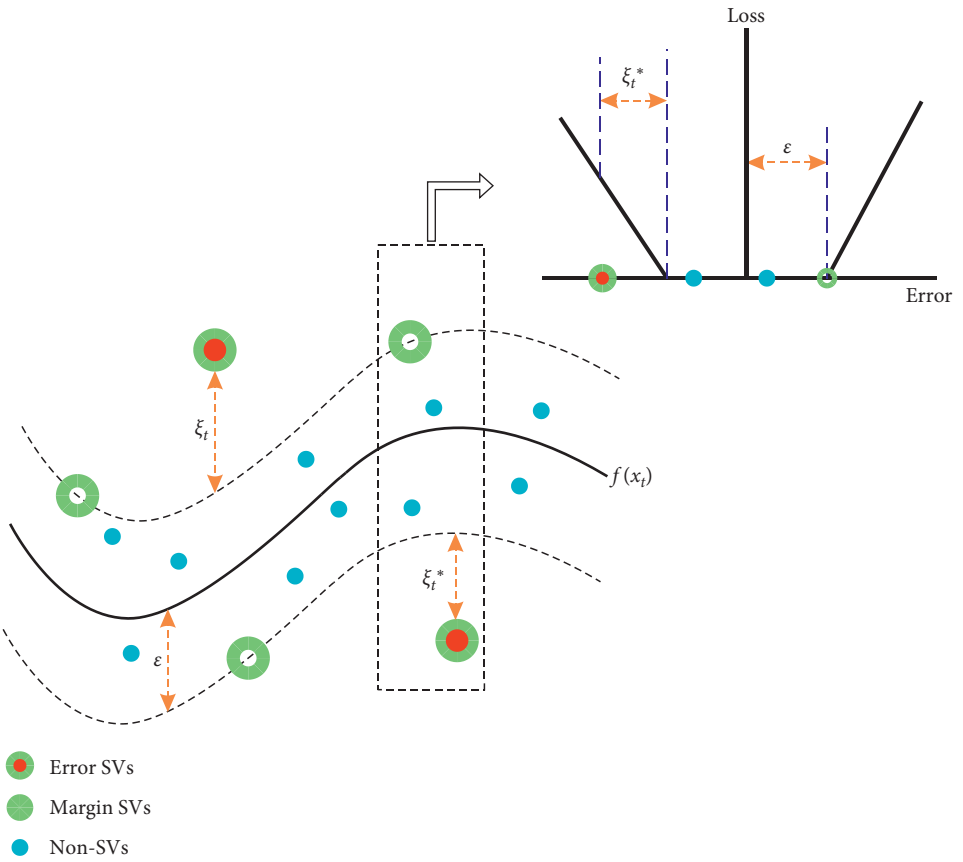

Figure 2: Nonlinear SVM regression with the ε-insensitive loss function.

Table 1: Popular kernel types.

Type	Kernel function	Remark
Linear	$K(x,z) = x^T z$	
Polynomial	$K(x,z) = (ax^T z + c)^d$	a is the scale, c is the offset, and d denotes the degree of the polynomial kernel (positive scalar).
tanh	$K(x,z) = \tanh(ax^T z + c)$	a is the scale (positive scalar), and c is the offset of the tanh kernel.
Gaussian	$K(x,z) = \exp[-((x-z)^2/2\sigma^2)]$	σ is the width of the Gaussian kernel (positive scalar).
ANOVA	$K(x,z) = \sum_{k=1}^{n} \exp[-\sigma(x^k - z^k)^2]^d$	σ is the width (positive scalar) and d denotes the degree of the kernel.
Bessel	$K(x,z) = (J_{v+1}(\sigma\|x-z\|))/(\|x-z\|^{-n(v+1)})$	σ is the width of the kernel, and J is the bessel function of the first kind.

$$\text{ACE} = \text{PICP} - \text{PINC}. \tag{17}$$

The mean prediction interval width (MPIW) measures the average width of the PIs and is derived as follows:

$$\text{MPIW} = \frac{1}{T}\sum_{t=1}^{T}\left|y_t^{\overline{\tau}} - y_t^{\underline{\tau}}\right|. \tag{18}$$

For a comparison of the PIs developed using different methods, the MPIW can be normalized by the range of the corresponding data set R. The normalized MPIW (NMPIW) measures the width degree of constructed PIs and is derived as follows:

$$\text{NMPIW} = \frac{\text{MPIW}}{R}. \tag{19}$$

From a practical standpoint, it is important to have narrow PIs (small MPIW and NMPIW) with a high coverage probability (large PICP) [54].

In this study, three indices including mean absolute error (MAE), mean absolute percentage error (MAPE), root mean square error (RMSE), and coefficient of determination (R^2)

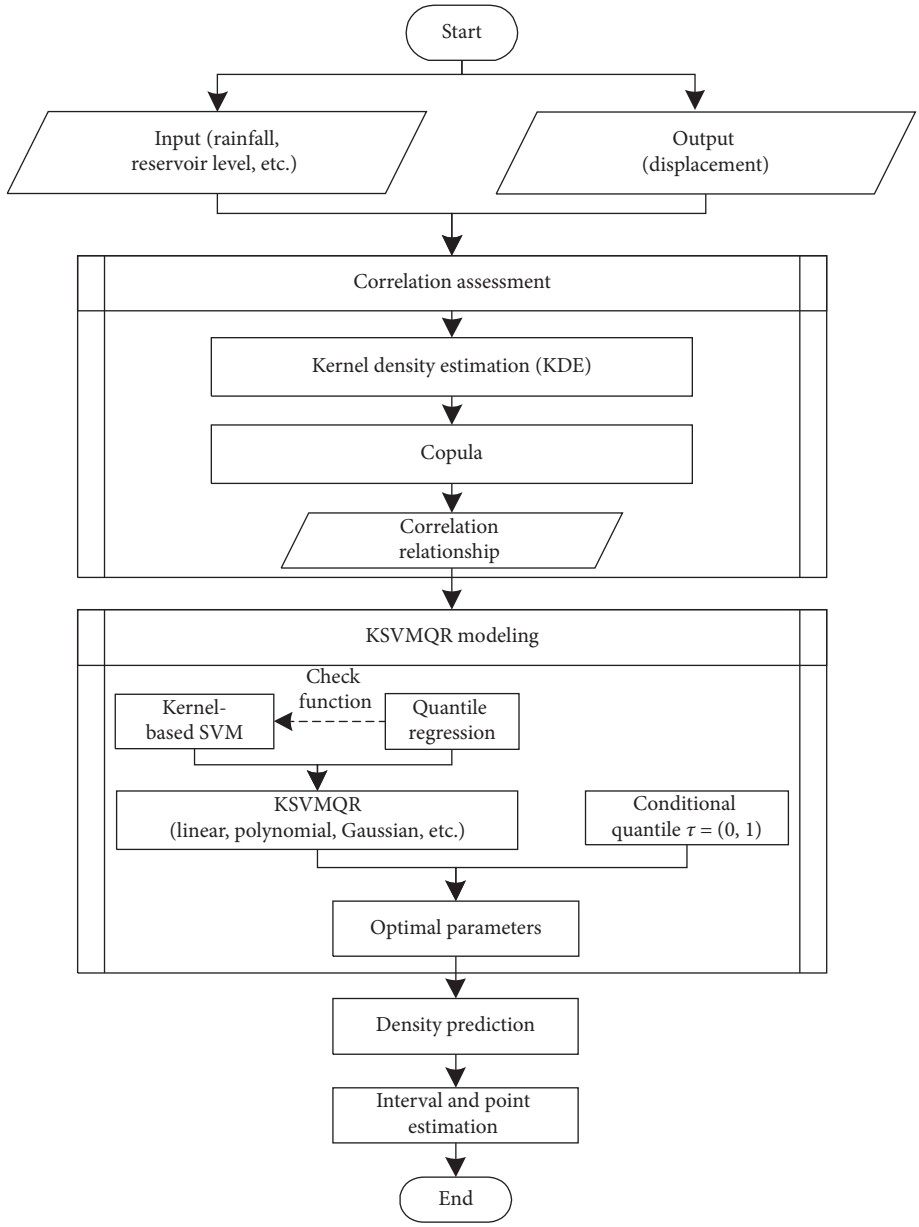

Figure 3: The overall framework of the density prediction for landslide displacement using the copula-KSVMQR approach.

Table 2: Selected publications on input selection using a computational intelligence approach for landslide displacement prediction.

Reference	Algorithm	Basis of input selection
[1]	Particle swarm-optimized support vector machine (PSO-SVM)	Experience, qualitative analysis
[23]	Bootstrap-ELM-ANN	Experience, literature review
[10]	Improved back propagation (BP) neural network	Experience
[11]	Chaotic model and extreme learning machine	Experience, qualitative analysis
[12]	Genetic algorithm and support vector machine (GA-SVM)	Experience, qualitative analysis
[13]	Particle swarm-optimized support vector machine (PSO-SVM)	Experience, qualitative analysis
[14]	Particle swarm-optimized support vector machine (PSO-SVM)	Experience, qualitative analysis, grey correlation analysis
[24]	Neural networks with random hidden weights	Experience
[47]	Polynomial regression and BP	Experience, qualitative analysis, literature review
[48]	Extreme learning machine (ELM)	Experience, qualitative analysis, grey correlation analysis

are used to assess the performance of point prediction. MAE, MAPE, and RMSE are defined as follows:

$$\begin{aligned} \text{MAE} &= \frac{1}{T}\left(\sum_{t=1}^{T}\left|\widehat{y}_t - y_t\right|\right), \\ \text{MAPE} &= \frac{1}{T}\left(\sum_{t=1}^{T}\left|\frac{\widehat{y}_t - y_t}{y_t}\right|\right) \times 100\%, \\ \text{RMSE} &= \sqrt{\frac{\sum_{t=1}^{T}\left(\widehat{y}_t - y_t\right)^2}{T}}, \\ R^2 &= \left[\frac{\sum_{t=1}^{T}\left(y_t - \overline{y}\right)\left(\widehat{y}_t - \overline{\widehat{y}}\right)}{\sqrt{\sum_{t=1}^{T}\left(y_t - \overline{y}\right)^2\left(\widehat{y}_t - \overline{\widehat{y}}\right)^2}}\right]^2, \end{aligned} \tag{20}$$

where $\widehat{y}_t$ and y_t denote the t-th predictive value and observation, respectively, and $\overline{y}$ and $\overline{\widehat{y}}$ denote the mean of the observation and predictive value.

3. Tanjiahe Landslide

3.1. Geological Setting. The Tanjiahe landslide (Figure 4(a)), a complex landslide in the TGRA, is located in Shazhenxi Town, Zigui County, Hubei Province. The landslide site is located on the right bank of the Yangtze River, approximately 56 km northwest of the Three Gorges Reservoir Dam (latitude and longitude coordinates: N31°01′53.9″, E110°30′26.9″, see Figure 4(b)). The landslide has a length of 1000 m, width of 400 m, average thickness of 40 m, and volume of 16 million m^3. The landslide toe is located at 135 m, and the crown is located at 432 m (Figure 4(c)). The slope surface consists of a gentle landform at the lower part and a comparatively steep landform at the upper part. The average inclinations for the upper and lower parts of the landslide surface are 25° and less than 10°, respectively. The main sliding direction of the landslide is 345°.

According to site investigation and borehole analysis, the landslide masses are arranged in two different layers (a colluvial gravel soil deposit and cataclastic rocks) (Figure 5). The colluvial gravel soil deposit is composed of silty clay and gravel clasts. The gravel clasts with diameters ranging from 0.2 to 10 cm represent approximately 60% of the deposit by weight. The colluvial gravel soil deposit is underlaid by cataclastic sandstone. The sliding zone with thickness ranging from 1.0 to 1.2 m is composed of magenta silty clay (representing 70% by weight) and gravel clasts (representing 30% by weight). The cataclastic sandstone is underlaid by carbonaceous sandstone and quartz sandstone of the Jurassic Xiangxi formation (J1x). The dip direction and dip angle of the sandstone are 10° and 36°, respectively. The site-specific investigation shows that the sandstones contain two discontinuity sets (215°∠73° and 110°∠86°). Soft coal layers are prevalent in the J1x formation, and many landslides deformed along the soft coal layers. The Tanjiahe landslide mass also slides along a soft coal layer.

3.2. Deformation Characteristics. The Tanjiahe landslide was suspended before September 2006. When the reservoir level reached 156 m, the landslide was found reactivated and cracks were observed by locals at the crown of the landslide. In July 2007, a collapse with a material volume of 300 m^2 occurred at an elevation of 350 m. A crack with length of 30 m and width of 20 cm was observed by the locals at an elevation of 350 m in August 2007. In September 2007, cracks were observed at elevations between 400 and 420 m, and the major crack reached approximately 150 m in length.

Four GPS monuments were established on the landslide mass for regular monitoring of the landslide deformations (see Figure 5 for locations). All GPS monuments were surveyed monthly. Figure 6 shows the rainfall intensity, the reservoir level, the reservoir fluctuations, the displacement, and velocity over the ten-year period between October 2006 and June 2015. The available data denote the following trends.

The Tanjiahe landslide is continuously deformed under the effect of reservoir water level fluctuation and rainfall. At the end of the monitoring period (June 2015), maximum displacement for ZG289, ZG288, ZG287, and ZG290 were values of 1775 mm, 1727 mm, 1692 mm, and 1163 mm, respectively. The displacements show that larger deformation occurred at the middle (ZG289 and ZG288) than at the crown (ZG287) than at the toe (ZG290).

When the reservoir level first reached a new high level of 175 m, the deformation velocity measured at ZG287 reached a value approximately 40 mm/month. Moreover, the landslide was reactivated by initially filling to 156 m. The results of the above analysis suggest that the correlations between the reservoir level and landslide displacement are significant.

In the dry season, from October of the current year to April of the following year, when the landslide area experienced little rainfall and the reservoir slightly dropped, the velocities at ZG287 showed an increasing downward trend. For example, such a case occurred during the dry season months of 2009, 2010, and 2011. However, in the rain season, from May to September, the velocities at ZG287 show a decreasing trend. These findings indicate that the correlations between the rainfall and landslide displacement are limited. Furthermore, a stronger correlation exists between reservoir fluctuations and landslide displacement.

3.3. Displacement Prediction Based on the Copula-KSVMQR Approach

3.3.1. Correlation Analysis. The above deformation analysis shows that significant movements occurred at the middle and rear of the landslide mass. Therefore, GPS monuments installed in the middle and upper parts, ZG289 and ZG287, were selected to establish a displacement prediction mode for the Tanjiahe landslide, and the measured displacement at ZG289 was chosen for the correlation analyses.

Based on previous studies of displacement prediction for reservoir landslide [1, 48], seven variables including four trigger variables and three state variables were considered as optional inputs (x_t), and displacement in the current month

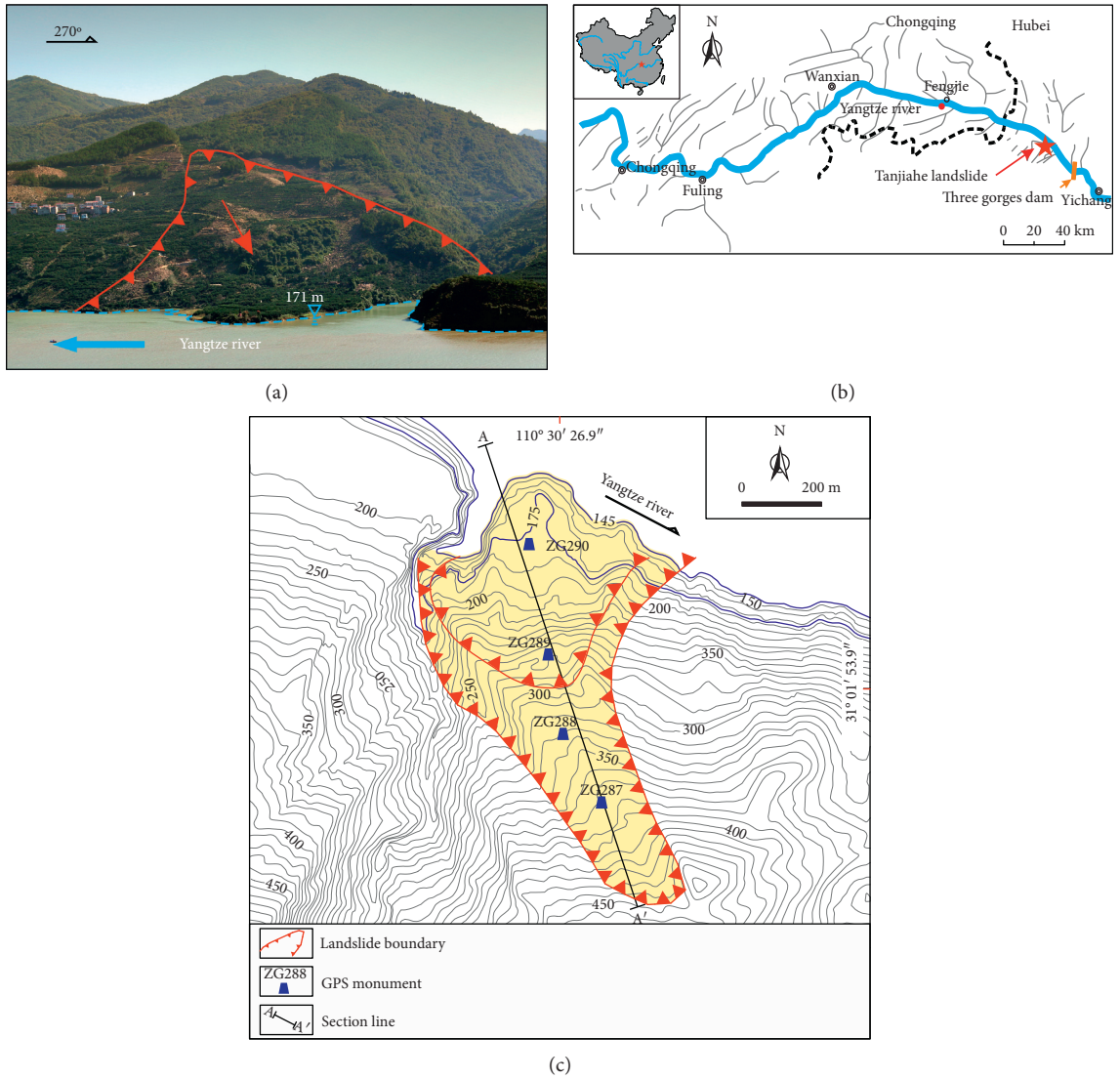

Figure 4: (a) Overall view of the Tanjiahe landslide. (b) Location of the Tanjiahe landslide, TGRA, China. (c) Topographic map of the Tanjiahe landslide.

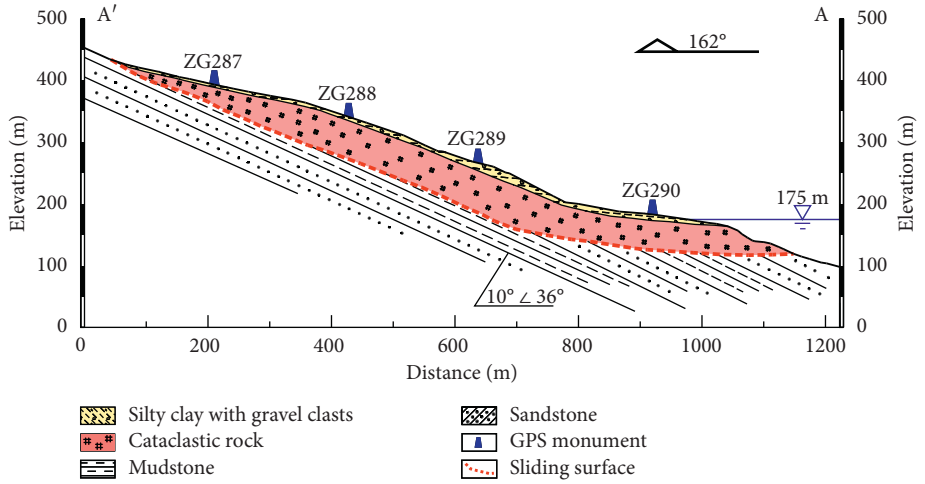

Figure 5: Geological profile along section A-A′ with monitoring instruments.

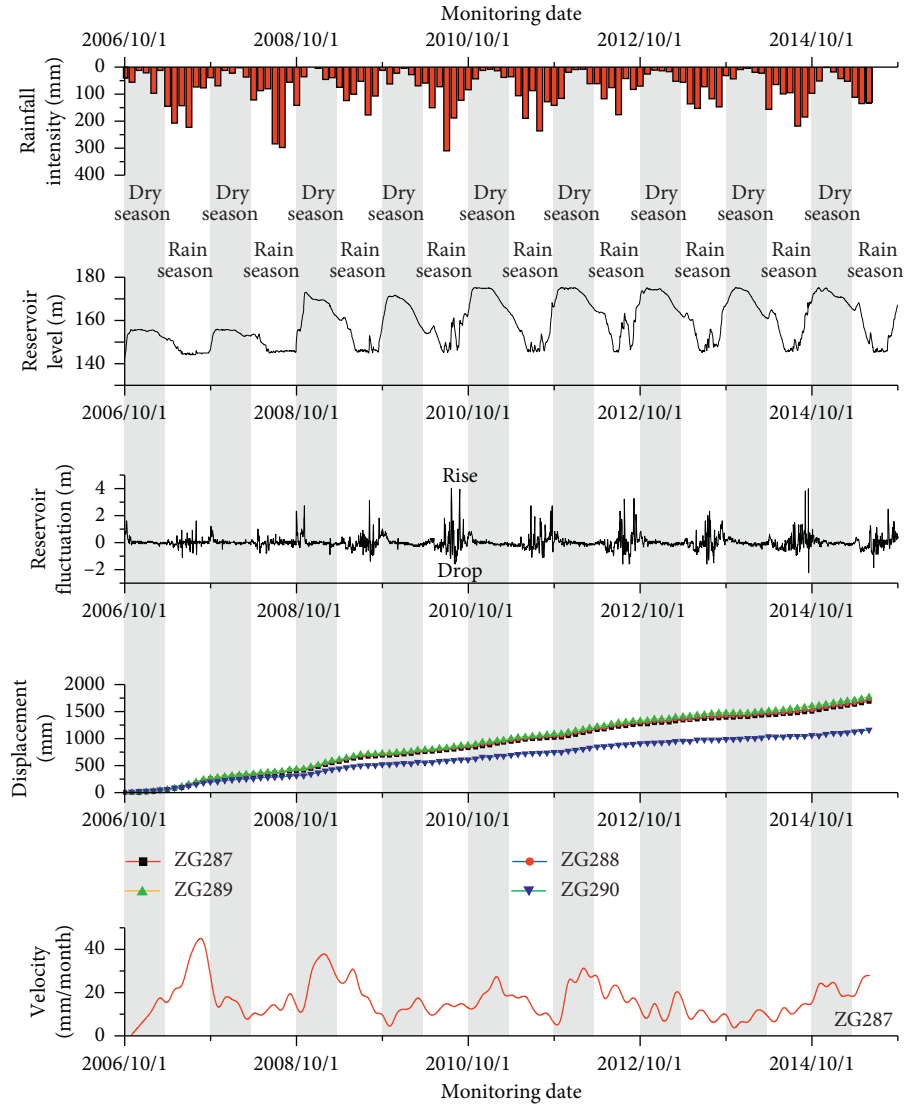

Figure 6: Time series of rainfall intensity, reservoir level, reservoir fluctuation, landslide displacement, and velocity obtained from the multisensor monitoring system spanning the period of October 2006 to June 2015.

(y_t) was chosen as the output. The four trigger variables consist of the rainfall intensity over the past month (x_t^1), the rainfall intensity over the past two months (x_t^2), the average reservoir level in the current month (x_t^3), and the variation in the reservoir level in the current month (x_t^4). The three state variables consist of the displacement over the past one month (x_t^5), the displacement over the past two months (x_t^6), and the displacement over the past three months (x_t^7).

The correlation relationships between the optional input and output variables were evaluated using copula analyses. The Gaussian kernel density estimation was first applied to obtain the marginal probability density function. The bandwidths of the Gaussian kernel density estimation for variables related to the rainfall, reservoir, and displacement were set to 0.05, 0.05, and 0.5, respectively. Student's t copula was chosen to identify the bivariate correlation between the input variables and landslide displacement. The obtained correlation coefficients between the optional input variables and output displacement are listed in Table 3, and the joint t-copula density functions between the rainfall, reservoir level, and reservoir fluctuation and the displacement are shown in Figure 7. The copula analysis clearly shows the correlation relationships between the input variables and output displacement. Very strong positive correlations with coefficients greater than 0.95 were observed between the three state factors $(x_t^5, x_t^6, \text{and } x_t^7)$ and the landslide

Table 3: Correlation coefficients between input variables and landslide displacement.

Bivariate	Kendall's tau	Spearman's rho	Remark
x_t^1, y_t	0.1215	0.1310	Weak positive
x_t^2, y_t	0.1218	0.1314	Weak positive
x_t^3, y_t	0.4055	0.5767	Strong positive
x_t^4, y_t	−0.2821	−0.3230	Moderate negative
x_t^5, y_t	0.9997	0.9873	Very strong positive
x_t^6, y_t	0.9994	0.9990	Very strong positive
x_t^7, y_t	0.9719	0.9989	Very strong positive

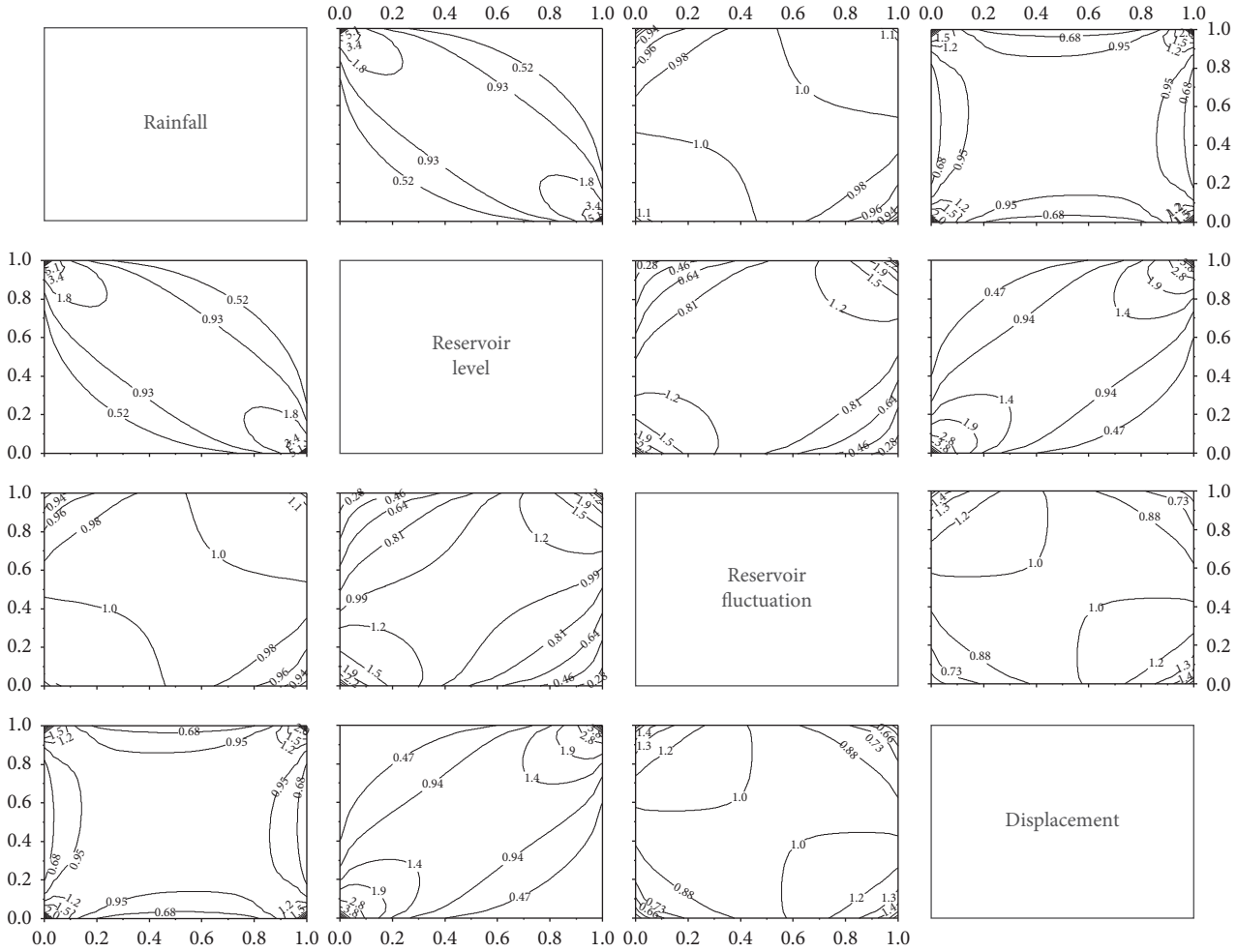

Figure 7: Cross sections of joint t-copula density between rainfall, reservoir level, reservoir fluctuation, and landslide displacement.

displacement, and a strong positive correlation with coefficients of 0.4055 and 0.5767 was noted between the reservoir level (x_t^3) and landslide displacement. The cross section of the joint t-copula density function between the reservoir level and landslide displacement (Figure 7) shows a heavy symmetric tail character that indicates that a strong correlation exists between the lower tail (0, 0) and upper tail (1, 1). In other words, the likelihood of a large displacement is relatively high when the reservoir reaches a high level. Additionally, a moderate negative correlation (Kendall's tau = −0.2821, Spearman's rho = −0.3230) was found between the reservoir fluctuation (x_t^4) and landslide displacement, suggesting that a negative fluctuation, referring to the drawdown of the reservoir, was more likely to cause positive landslide movement. The cross section of the joint t-copula density between the reservoir fluctuation and displacement (Figure 7) implies that a moderate correlation exists between points (0, 1) and (1, 0). Additionally, correlation coefficients greater than 0.1 indicate weak positive correlations between the rainfall variables (x_t^1 and x_t^2) and landslide displacement. The cross section of the joint t-copula density between the rainfall and displacement (Figure 7) implies a thinner tail than those for the reservoir level. The above results indicate that weak to strong correlations were found between the selected optional input variables and output displacement, and thus, the seven optional inputs were adopted in the following process. These results are consistent with the results of field observations.

3.3.2. KSVMQR Modeling. The landslide monitoring data were first normalized in the range of 0 to 1 by the unity-based normalization (or min-max feature scaling). The landslide displacement predictions were obtained after renormalizing the outputs from the KSVMQR approach. Monitoring data from October 2006 to December 2014 were treated as training data, and the remaining monitoring data were treated as testing data. Six KSVMQR models with different kernels for $\tau = 0.01, 0.02, \ldots, 0.98, 0.99$ with an interval of 0.01 were trained for GPS monuments ZG287 and ZG289. The parameters used to train the KSVMQR models with the different kernels are listed in Table 4. Those simulations were performed in RStudio Version 1.1.383 running on an Intel(R) Xeon(R) E-2176M @ 2.70 GHz CPU with 64 GB RAM.

Table 4: Parameters used in the KSVMQR model with different kernels.

Kernel type	Parameters
Polynomial	$a = 1$, $c = 1$, $d = 2$
Linear	—
tanh	$a = 0.02$, $c = 1$
Gaussian	$\sigma = 0.05$
ANOVA	$\sigma = 1$, $d = 1$
Bessel	$\sigma = 1$, $d = 1$

3.4. Results. The performance indices for the KSVMQR models with different kernels are listed in Table 5. The obtained results show that the proposed approach is sensitive to the choice of the kernel type. The evaluation metrics for point prediction (MAE, MAPE, RMSE) and interval prediction (PICP, ACE, MPIW, NMPIW) indicate that the polynomial KSVMQR model provided the best result compared with the KSVMQR models with linear, tanh, Gaussian, ANOVA, and Bessel kernels. Therefore, the polynomial KSVMQR model was chosen to construct density prediction of the Tanjiahe landslide.

3.4.1. Density Prediction. The complete probability density distributions of landslide predictions based on the polynomial KSVMQR at ZG287 and ZG289 spanning the period of January 2015 to June 2015 are shown in Figures 8 and 9. The density distribution distributions look quite different from a uniform distribution. We can see that all observations are located almost in the middle of the density distributions, especially for the predictions of February, March, and April at ZG287 and ZG289. Meanwhile, it can be seen that the observations mostly lie within the predictive distribution with high probability, expect for observations of June. The small fraction falling into the tail of the probability density curve is because with the lengthening of the forecasting period, there are more uncertainties associated with landslide predictions.

3.4.2. Interval Prediction. The constructed PIs with a PINC of 90% obtained from the $\widehat{y}_t^{\tau=0.05}$ and $\widehat{y}_t^{\tau=0.95}$ quantile predictions are shown in Figure 10. The corresponding evaluation indices including PICP, ACE, MPIW, and NMPIW are listed in Table 5. As shown, narrow PIs (small MPIW and NMPIW) were obtained, and the constructed PIs based on the polynomial KSVMQR cover the observations completely, with percentages of 100%. These results indicate that reliable PIs with satisfactory performance were constructed.

3.4.3. Point Prediction. Figure 11 shows the obtained point predictions generated from median predictions ($\widehat{y}_t^{\tau=0.5}$). It can be seen that the obtained point predictions show great consistency with the observations, with correlation coefficients of 0.9998. For example, the generated point predictions for monitoring point ZG289 have MAE, MAPE, RMSE, and R^2 values of 6.39, 2.27, 8.70, and 0.9998, respectively. Therefore, the polynomial KSVMQR models provide very good point predictions for the Tanjiahe landslide. To further evaluate the performance of the copula-KSVMQR, comparative analyses were conducted with the traditional algorithms including Bootstrap-ELM-ANN, BP, radial basis function (RBF), ELM, and SVM.

From the view of interval prediction, the constructed PIs based on the polynomial KSVMQR approach have a smaller MPIW and NMPIW compared with Bootstrap-ELM-ANN. The above result indicates that the polynomial KSVMQR approach outperforms the persistence Bootstrap-ELM-ANN method in terms of interval prediction. For example, the MPIW for 90% PI at ZG289 was 33.04, which is approximately 60 percent lower than that obtained using the traditional Bootstrap-ELM-ANN. Furthermore, any desired confidence level (e.g., 90%, 80%, or 50%) can be derived from the density prediction using the copula-KSVMQR approach. Conversely, given only a 90% interval prediction, there is no way to infer a density prediction.

From the view of point prediction, the evaluation metrics of point prediction including MAE, MAPE, and RMSE indicate that the median prediction of the polynomial KSVMQR approach provides equivalent predictions to the SVM. The median prediction of the polynomial KSVMQR approach only outperforms the SVM at ZG289. Although the median prediction of the polynomial KSVMQR provides lower performance than the SVM at ZG289, in the MAE, MAPE, and RMSE, it outperforms the traditional BP, RBF, and ELM for both ZG287 and ZG289. These performance differences are mainly because the same KSVMQ model parameters listed in Table 4 were applied for both ZG287 and ZG289. However, different optimization model parameters obtained from particle swarm optimization were applied for ZG287 and ZG289. These results indirectly indicate that the proposed approach is less sensitive to the model parameters compared with the SVM.

Moreover, several polynomial KSVMQR models with different numbers of quantiles were trained to further verify the robustness of the proposed approach. The interval performance index MPIWs for the 90% PIs of ZG289 with an increasing number of quantiles in KSVMQR are shown in Figure 12. The obtained performance indices clearly show that MPIWs of 90% PIs at ZG289 remain steady with the increasing number of quantiles which indicates that stable PI was achieved even with different quantile intervals. Therefore, the copula-KSVMQR approach is considered to be robust.

In general, the proposed hybrid approach needs to train models of multiple quantiles to construct the complete probability distributions. Computational time is an important issue that should be considered. Figure 12 shows the required computational time with the increasing number of quantiles in KSVMQR at monitoring point ZG289. Simulations were performed in RStudio Version 1.1.383 running on an Intel(R) Xeon(R) E-2176M @ 2.70 GHz CPU with 64 GB RAM. It can be seen that the required computational time is highly related to the number of quantiles. Moreover, even to train 9999 quantile predictions, the required computation time is approximately 69.17 s. Thus, the approach is computationally efficient.

Table 5: Performance indices for the predictions of the Tanjiahe landslide.

Monitoring point	Method	PINC (%)	PICP (%)	ACE (%)	MPIW (mm)	NMPIW	MAE (mm)	MAPE (%)	RMSE (mm)
ZG287	Copula-KSVMQR (polynomial)	90	100	10	27.30	0.0162	6.39	3.06	9.31
	Copula-KSVMQR (linear)	90	86.67	−3.33	38.15	0.0226	6.71	4.14	9.51
	Copula-KSVMQR (tanh)	90	83.81	−6.19	1342.81	0.7953	18.54	10.26	24.88
	Copula-KSVMQR (Gaussian)	90	85.71	−4.29	44.91	0.0266	11.59	15.11	17.23
	Copula-KSVMQR (ANOVA)	90	81.90	−8.1	36.82	0.0218	7.73	3.97	11.62
	Copula-KSVMQR (bessel)	90	84.76	−5.24	42.57	0.0252	11.80	17.12	17.51
	Bootstrap-ELM-ANN	90	100	10	68.71	0.0407	—	—	—
	BP	—	—	—	—	—	9.31	3.38	17.48
	RBF	—	—	—	—	—	15.78	1.85	49.10
	ELM	—	—	—	—	—	8.57	2.23	14.93
	SVM	—	—	—	—	—	5.62	1.30	7.80
ZG289	Copula-KSVMQR (polynomial)	90	100	10	33.04	0.0187	6.47	1.35	8.75
	Copula-KSVMQR (linear)	90	86.27	−3.73	39.44	0.0223	7.67	1.65	10.00
	Copula-KSVMQR (tanh)	90	87.25	−2.75	44.69	0.0252	11.31	3.79	16.68
	Copula-KSVMQR (Gaussian)	90	86.27	−3.73	1429.73	0.8072	20.78	6.60	26.31
	Copula-KSVMQR (ANOVA)	90	45.10	−44.9	20.40	0.0115	18.24	3.95	25.25
	Copula-KSVMQR (bessel)	90	45.10	−44.9	20.40	0.0115	11.55	4.42	17.20
	Bootstrap-ELM-ANN	90	100	10	80.63	0.0455	—	—	—
	BP	—	—	—	—	—	9.14	1.78	15.80
	RBF	—	—	—	—	—	16.02	1.58	51.73
	ELM	—	—	—	—	—	9.91	2.44	12.45
	SVM	—	—	—	—	—	7.18	1.19	9.39

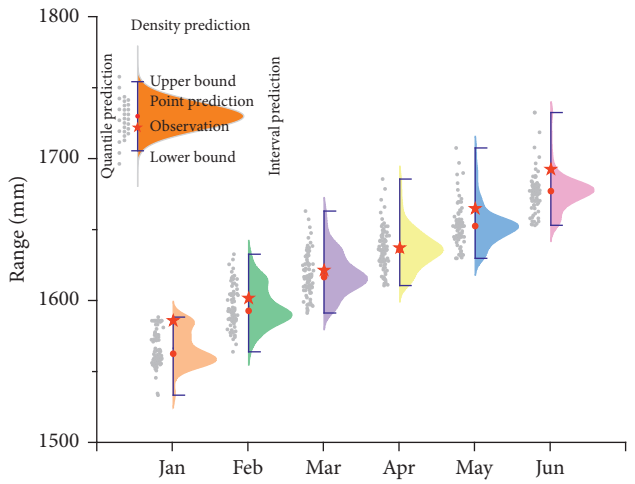

Figure 8: Probability density distribution of predictive displacement based on polynomial KSVMQR at ZG287 spanning the period of January 2015 to June 2015.

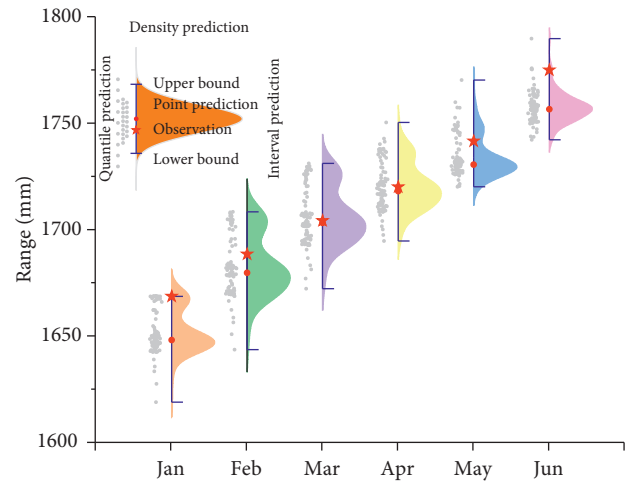

Figure 9: Probability density distribution of predictive displacement based on polynomial KSVMQR at ZG289 spanning the period of January 2015 to June 2015.

4. Discussion

In the present study, the density regression functions between causal factors, including four trigger variables and three state variables, and landslide displacement were trained based on historical monitoring data using the copula-KSVMQR approach. The trained density models can be easily updated based on new and more recent data to predict further landslide displacement. The advantage of the copula-KSVMQ-based density prediction is that it conveys

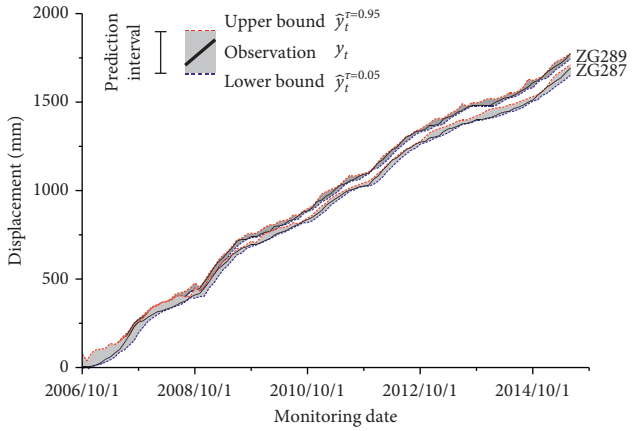

Figure 10: PIs with a nominal confidence level of 90% for landslide displacement obtained using the polynomial KSVMQR.

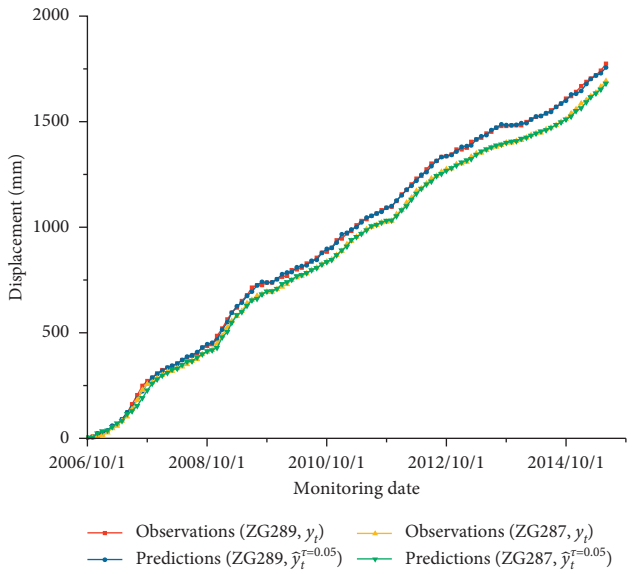

Figure 11: Comparisons of the median predictions ($\hat{y}_t^{\tau=0.5}$) and observations for ZG 287 and ZG289.

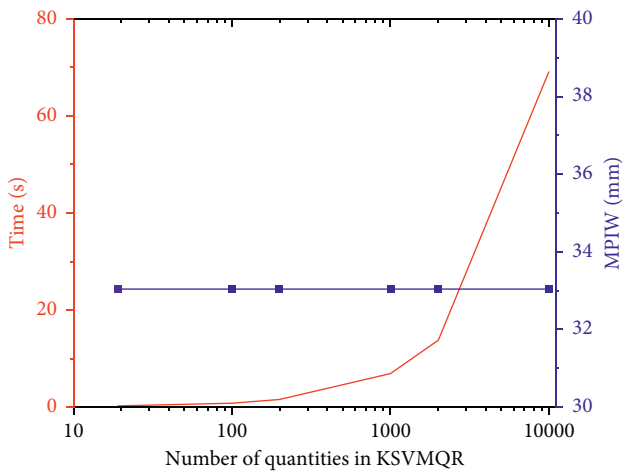

Figure 12: The required computational time and MPIW of constructed 90% PIs of ZG289 with an increasing number of quantiles in KSVMQR.

more information and offers an estimate of the future probability distribution of landslide displacement, conditional on the information available at the time the prediction is made. This may suggest that density predictions are preferred. However, due to the more advanced and intensive computational methods that are required, density prediction is still in its initial stage.

To summarize, the advantages of probability density prediction based on the copula-KSVMQR approach are outlined as follows:

Complete probability distributions of predictions are provided. Meanwhile, the landslide observations lie within the predictive distribution with high probability. Moreover, a wide range of accuracy predictions, including interval and deterministic point predictions, can be derived from the complete predictive distribution. The hybrid approach appears to be computationally efficient and robust. It is also less parameter-sensitive than the traditional SVM algorithm; thus, it is easier to apply.

Nevertheless, probability density prediction based on the copula-KSVMQR also has some disadvantages, the main one being the lack of transparency of the trained model. The proposed approach behaves as a black box, and therefore, the interpretation of the model is almost impossible. In addition, selection of the suitable kernel function, which is significant for the quality of the trained model, is a trial and error process. Moreover, a high level of knowledge on advanced and intensive computational methods is required to train multiple quantile models.

5. Conclusions

Density prediction offering a full probability density distribution of landslide displacement is promising for landslide early warning and mitigation. A hybrid computational intelligence approach using the copula-KSVMQR method was proposed in the present study to build a prediction model of landslide displacement and construct the density distribution of the landslide displacement prediction. The hybrid copula-KSVMQR approach is successfully applied to a complex landslide in the TGRA. The experimental study indicates that the proposed copula-KSVMQR approach achieves perfect performance. Density predictions with full probability density distributions of the landslide displacement can be constructed from the copula-KSVMQR approach. Landslide observations were found in the middle of the probability density distribution with high probability. In addition, different types of predictions, including interval prediction and point prediction, can be derived from the obtained density prediction with perfect performance. The constructed PIs cover the observations completely and appropriately account for all uncertainties. The mean prediction interval width of the proposed approach at ZG 289 is 33.04, which is approximately 60 percent lower than that obtained using the traditional Bootstrap-ELM-ANN. The deterministic point prediction and observations showed good consistency with correlation coefficients of 0.9998. The results obtained for the Tanjiahe landslide indicate that the copula-

KSVMQR approach is effective and efficient in landslide displacement prediction.

Data Availability

The data used in this study are available from the corresponding author upon reasonable request.

Conflicts of Interest

The authors declare no conflicts of interest.

Acknowledgments

This study was financially supported by the National Key R&D Program of China (Grant no. 2018YFC1507200), the National Natural Science Foundation of China (Grant nos. 41702328 and 41827808), Hubei Provincial Natural Science Foundation of China (Grant no. 2019CFB585), and the Fundamental Research Funds for the Central Universities, China University of Geosciences (Wuhan) (Grant nos. CUGL170813 and CUGQYZX1747). All support is gratefully acknowledged.

References

[1] C. Zhou, K. Yin, Y. Cao, and B. Ahmed, "Application of time series analysis and PSO-SVM model in predicting the Bazimen landslide in the Three Gorges Reservoir, China," *Engineering Geology*, vol. 204, pp. 108–120, 2016.

[2] W. Yao, Z. Zeng, C. Lian, and H. Tang, "Training enhanced reservoir computing predictor for landslide displacement," *Engineering Geology*, vol. 188, no. 0, pp. 101–109, 2015.

[3] S.-H. Jiang, J. Huang, C. Yao, and J. Yang, "Quantitative risk assessment of slope failure in 2-D spatially variable soils by limit equilibrium method," *Applied Mathematical Modelling*, vol. 47, pp. 710–725, 2017.

[4] S.-H. Jiang and J.-S. Huang, "Efficient slope reliability analysis at low-probability levels in spatially variable soils," *Computers and Geotechnics*, vol. 75, pp. 18–27, 2016.

[5] S. Jiang, M. J. Lian, C. W. Lu, Q. H. Gu, S. L. Ruan, and X. C. Xie, "Ensemble prediction algorithm of anomaly monitoring based on big data analysis platform of open-pit mine slope," *Complexity*, vol. 2018, Article ID 1048756, 13 pages, 2018.

[6] J. Ma, H. Tang, X. Hu et al., "Identification of causal factors for the Majiagou landslide using modern data mining methods," *Landslides*, vol. 14, no. 1, pp. 311–322, 2017.

[7] D. Tang, D.-Q. Li, and Z.-J. Cao, "Slope stability analysis in the Three Gorges Reservoir Area considering effect of antecedent rainfall," *Georisk: Assessment and Management of Risk for Engineered Systems and Geohazards*, vol. 11, no. 2, pp. 161–172, 2017.

[8] M. Saito, "Forecasting the time of occurrence of a slope failure," in *Proceedings of 6th International Congress of Soil Mechanics and Foundation Engineering*, pp. 537–541, Montreal, Canada, 1965.

[9] J. Ma, H. Tang, X. Liu, X. Hu, M. Sun, and Y. Song, "Establishment of a deformation forecasting model for a step-like landslide based on decision tree C5.0 and two-step cluster algorithms: a case study in the Three Gorges Reservoir area, China," *Landslides*, vol. 14, no. 3, pp. 1275–1281, 2017.

[10] H. Chen and Z. Zeng, "Deformation prediction of landslide based on improved back-propagation neural network," *Cognitive Computation*, vol. 5, no. 1, pp. 56–62, 2012.

[11] F. Huang, J. Huang, S. Jiang, and C. Zhou, "Landslide displacement prediction based on multivariate chaotic model and extreme learning machine," *Engineering Geology*, vol. 218, pp. 173–186, 2017.

[12] X. Z. Li and J. M. Kong, "Application of GA-SVM method with parameter optimization for landslide development prediction," *Natural Hazards and Earth System Sciences*, vol. 14, no. 3, pp. 525–533, 2014.

[13] F. Ren, X. Wu, K. Zhang, and R. Niu, "Application of wavelet analysis and a particle swarm-optimized support vector machine to predict the displacement of the Shuping landslide in the Three Gorges, China," *Environmental Earth Sciences*, vol. 73, no. 8, pp. 4791–4804, 2014.

[14] T. Wen, H. Tang, Y. Wang, C. Lin, and C. Xiong, "Landslide displacement prediction using the GA-LSSVM model and time series analysis: a case study of Three Gorges Reservoir, China," *Natural Hazards and Earth System Sciences*, vol. 17, no. 12, pp. 2181–2198, 2017.

[15] S. Xu and R. Niu, "Displacement prediction of Baijiabao landslide based on empirical mode decomposition and long short-term memory neural network in Three Gorges area, China," *Computers & Geosciences*, vol. 111, pp. 87–96, 2018.

[16] H. Li, Q. Xu, Y. He, X. Fan, and S. Li, "Modeling and predicting reservoir landslide displacement with deep belief network and EWMA control charts: a case study in Three Gorges Reservoir," *Landslides*, pp. 1–15, 2019.

[17] F. M. Huang, K. L. Yin, G. R. Zhang, L. Gui, B. B. Yang, and L. Liu, "Landslide displacement prediction using discrete wavelet transform and extreme learning machine based on chaos theory," *Environmental Earth Sciences*, vol. 75, no. 20, p. 1376, 2016.

[18] A. Elshorbagy, G. Corzo, S. Srinivasulu, and D. P. Solomatine, "Experimental investigation of the predictive capabilities of data driven modeling techniques in hydrology - Part 1: concepts and methodology," *Hydrology and Earth System Sciences*, vol. 14, no. 10, pp. 1931–1941, 2010.

[19] A. Elshorbagy, G. Corzo, S. Srinivasulu, and D. P. Solomatine, "Experimental investigation of the predictive capabilities of data driven modeling techniques in hydrology—part 2: Application," *Hydrology and Earth System Sciences*, vol. 14, no. 10, pp. 1943–1961, 2010.

[20] K. S. Kasiviswanathan, K. P. Sudheer, and J. He, "Quantification of prediction uncertainty in artificial neural network models," in *Artificial Neural Network Modelling*, pp. 145–159, Springer, Berlin, Germany, 2016.

[21] K. S. Kasiviswanathan, J. He, K. P. Sudheer, and J.-H. Tay, "Potential application of wavelet neural network ensemble to forecast streamflow for flood management," *Journal of Hydrology*, vol. 536, pp. 161–173, 2016.

[22] K. S. Kasiviswanathan and K. P. Sudheer, "Quantification of the predictive uncertainty of artificial neural network based river flow forecast models," *Stochastic Environmental Research and Risk Assessment*, vol. 27, no. 1, pp. 137–146, 2013.

[23] J. Ma, H. Tang, X. Liu et al., "Probabilistic forecasting of landslide displacement accounting for epistemic uncertainty: a case study in the Three Gorges Reservoir area, China," *Landslides*, vol. 15, no. 6, pp. 1145–1153, 2018.

[24] C. Lian, Z. Zeng, W. Yao, H. Tang, and C. L. P. Chen, "Landslide displacement prediction with uncertainty based on neural networks with random hidden weights," *IEEE Transactions on Neural Networks and Learning Systems*, vol. 27, no. 12, pp. 2683–2695, 2016.

[25] W. Yao, Z. Zeng, and C. Lian, "Generating probabilistic predictions using mean-variance estimation and echo state network," *Neurocomputing*, vol. 219, pp. 536–547, 2017.
[26] Y. Wang, H. Tang, T. Wen, and J. Ma, "A hybrid intelligent approach for constructing landslide displacement prediction intervals," *Applied Soft Computing*, vol. 81, p. 105506, 2019.
[27] A. Sklar, *Fonctions de Repartition an Dimensions et Leurs Marges*, Vol. 8, Paris Institute of Statistics, Paris, France, 1959.
[28] R. B. Nelsen, *An Introduction to Copulas*, Springer Science & Business Media, Berlin, Germany, 2007.
[29] X.-S. Tang, D.-Q. Li, G. Rong, K.-K. Phoon, and C.-B. Zhou, "Impact of copula selection on geotechnical reliability under incomplete probability information," *Computers and Geotechnics*, vol. 49, pp. 264–278, 2013.
[30] X.-S. Tang, D.-Q. Li, C.-B. Zhou, and K.-K. Phoon, "Copula-based approaches for evaluating slope reliability under incomplete probability information," *Structural Safety*, vol. 52, pp. 90–99, 2015.
[31] S. Huang, P. Li, Q. Huang, and G. Leng, "Copula-based identification of the non-stationarity of the relation between runoff and sediment load," *International Journal of Sediment Research*, vol. 32, no. 2, pp. 221–230, 2017.
[32] D. E. Kayalar, C. C. Küçüközmen, and A. S. Selcuk-Kestel, "The impact of crude oil prices on financial market indicators: copula approach," *Energy Economics*, vol. 61, pp. 162–173, 2017.
[33] J. Munkhammar, J. Widén, and L. M. Hinkelman, "A copula method for simulating correlated instantaneous solar irradiance in spatial networks," *Solar Energy*, vol. 143, pp. 10–21, 2017.
[34] H. Zhu, L. M. Zhang, T. Xiao, and X. Y. Li, "Generation of multivariate cross-correlated geotechnical random fields," *Computers and Geotechnics*, vol. 86, pp. 95–107, 2017.
[35] Z. Qin, W. Li, and X. Xiong, "Estimating wind speed probability distribution using kernel density method," *Electric Power Systems Research*, vol. 81, no. 12, pp. 2139–2146, 2011.
[36] S. Demarta and A. J. McNeil, "The t copula and related copulas," *International Statistical Review/Revue Internationale de Statistique*, vol. 73, no. 1, pp. 111–129, 2005.
[37] H. Akoglu, "User's guide to correlation coefficients," *Turkish Journal of Emergency Medicine*, vol. 18, no. 3, pp. 91–93, 2018.
[38] P. Schober, C. Boer, and L. A. Schwarte, "Correlation coefficients: appropriate use and interpretation," *Anesthesia & Analgesia*, vol. 126, no. 5, 2018.
[39] F. Lu, Z. Chen, W. Liu, and H. Shao, "Modeling chlorophyll-a concentrations using an artificial neural network for precisely eco-restoring lake basin," *Ecological Engineering*, vol. 95, pp. 422–429, 2016.
[40] R. Koenker and G. Bassett, "Regression quantiles," *Econometrica*, vol. 46, no. 1, pp. 33–50, 1978.
[41] H. Zhu, Y. Guo, W. You, and Y. Xu, "The heterogeneity dependence between crude oil price changes and industry stock market returns in China: evidence from a quantile regression approach," *Energy Economics*, vol. 55, no. Supplement C, pp. 30–41, 2016.
[42] C. Cortes and V. Vapnik, "Support-vector networks," *Machine Learning*, vol. 20, no. 3, pp. 273–297, 1995.
[43] H. Yang, L. Chan, and I. King, "Support vector machine regression for volatile stock market prediction," in *Intelligent Data Engineering and Automated Learning—IDEAL 2002*, H. Yin, N. Allinson, R. Freeman et al., Eds., pp. 391–396, Springer Berlin Heidelberg, Berlin, Heidelberg, 2002.
[44] C.-C. Chuang, S.-F. Su, J.-T. Jeng, and C.-C. Hsiao, "Robust support vector regression networks for function approximation with outliers," *IEEE Transactions on Neural Networks*, vol. 13, no. 6, pp. 1322–1330, 2002.
[45] Y. Huang and L. Zhao, "Review on landslide susceptibility mapping using support vector machines," *CATENA*, vol. 165, pp. 520–529, 2018.
[46] H. Wei, M. M. Wang, B. Y. Song, X. Wang, and D. L. Chen, "Study on the magnitude of reservoir-triggered earthquake based on support vector machines," *Complexity*, vol. 2018, Article ID 2830690, 10 pages, 2018.
[47] J. Du, K. Yin, and S. Lacasse, "Displacement prediction in colluvial landslides, Three Gorges Reservoir, China," *Landslides*, vol. 10, no. 2, pp. 203–218, 2013.
[48] Y. Cao, K. Yin, D. E. Alexander, and C. Zhou, "Using an extreme learning machine to predict the displacement of step-like landslides in relation to controlling factors," *Landslides*, vol. 13, no. 4, pp. 725–736, 2016.
[49] Y. Q. Zhang, *A Feature-Based Well Completion Optimization System Applying Fuzzy MCDM*, University of Alberta, Alberta, Canada, 2018.
[50] J. Zhou, Y. Y. Wang, F. Xiao, Y. Y. Wang, and L. J. Sun, "Water quality prediction method based on IGRA and LSTM," *Water*, vol. 10, no. 9, 2018.
[51] F. Golestaneh, P. Pinson, and H. B. Gooi, "Very short-term nonparametric probabilistic forecasting of renewable energy generation- with application to solar energy," *IEEE Transactions on Power Systems*, vol. 31, no. 5, pp. 3850–3863, 2016.
[52] C. Wan, J. Lin, J. Wang, Y. Song, and Z. Y. Dong, "Direct quantile regression for nonparametric probabilistic forecasting of wind power generation," *IEEE Transactions on Power Systems*, vol. 32, no. 4, pp. 2767–2778, 2017.
[53] B. D. Liu, J. Nowotarski, T. Hong, and R. Weron, "Probabilistic load forecasting via quantile regression averaging on sister forecasts," *IEEE Transactions on Smart Grid*, vol. 8, no. 2, pp. 730–737, 2017.
[54] C. Wan, Z. Xu, P. Pinson, Z. Y. Dong, and K. P. Wong, "Probabilistic forecasting of wind power generation using extreme learning machine," *IEEE Transactions on Power Systems*, vol. 29, no. 3, pp. 1033–1044, 2014.